Scripta Materialia 159 (2019) 85–88

Contents lists available at ScienceDirect

Scripta Materialia

journal homepage: www.elsevier.com/locate/scriptamat

Crack propagation mechanisms of an aged nickel-titanium-hafnium shape memory alloy

Behnam Amin-Ahmadi [a,*], Ronald D. Noebe [b], Aaron P. Stebner [a]

[a] Mechanical Engineering, Colorado School of Mines, Golden, CO 80401, USA
[b] NASA Glenn Research Center, Materials and Structures Division, Cleveland, OH 44135, USA

ARTICLE INFO

Article history:
Received 14 August 2018
Accepted 13 September 2018
Available online xxxx

Keywords:
Shape memory alloys (SMA)
Martensitic phase transformation
Twinning
Crack propagation
Transmission electron microscopy (TEM)

ABSTRACT

Mechanisms of crack propagation in a NiTiHf sample were studied from post-mortem microstructure characterizations about cracks. Transmission electron microscopy (TEM) analysis showed that a crack propagated within a martensite band along ⟨011⟩ type II twin planes. The crack was observed to switch between different twin planes to avoid precipitates. The crack tip terminated outside of the martensite band, within surrounding austenite. Amorphization of crack edges in both austenite and martensite was also detected, together with Ni enrichment. High-resolution TEM examination of crack tip inside the austenite phase also confirmed the formation of martensite nanocrystals embedded in the amorphous regions.

© 2018 Acta Materialia Inc. Published by Elsevier Ltd. All rights reserved.

Nickel-titanium-hafnium (NiTiHf) alloys have received considerable attention for their use as high-temperature shape memory alloys (SMAs). They can exhibit stable shape memory effect and superelastic behavior resulting from a solid-state phase transformation from high-temperature B2 austenite to low-temperature B19′ martensite through temperature change or applied stress [1,2]. An advantage of NiTiHf alloys is that the predicted stresses for slip are greater than that for twinning in the solid solution compounds [3], and the slip stresses can be driven even higher with H-phase nanoprecipitate strengthening via aging treatments [2,4]. This is why martensitic phase transformations of NiTiHf alloys are highly reversible while they exhibit little or no plastic deformation [1,2,5–8], which has been key to their emerging commercialization.

Due to the increased focus of NiTiHf alloys in medical and aerospace applications, cyclic thermo-mechanical durability and fracture resistance is highly desired. As a result, fundamental understanding of crack propagation in NiTiHf alloys is essential, though most studies on these systems have not included a detailed understanding of failure processes. In binary NiTi alloys, efforts have been made to understand the fundamental mechanisms of phase transformations [9–11], defect accumulation on cycling [12–15], and fracture [16–19]. From these studies, it is known that transformation toughening occurs as a result of stress-induced martensitic transformation accompanying crack growth in initially austenitic materials. However, there is a limited understanding of how microstructure affects the propagation of cracks in the low crystallographic symmetry martensite phases. Such understanding of fracture behavior in martensites is important to inform damage models for SMAs, which currently focus primarily on the role played by the dissipative mechanism of stress-induced phase transformation on crack growth [20–22], while ignoring phenomena related to the martensite phase itself. Through detailed TEM analysis, the present study documents crack propagation behavior within the martensite phase both near and away from strengthening nanoprecipitates, as well as observations of stress-induced amorphization around the crack tip inside both austenite and martensite phases in NiTiHf alloys.

A NiTiHf alloy with target composition of $Ni_{50.3}Ti_{41.2}Hf_{8.5}$ (at.%) was initially solution-annealed at 1050 °C for 30 min, water quenched, and then aged at 550 °C for 3.5 h and air-cooled to grow strengthening H-phase nanoprecipitates [4]. The samples were encapsulated in a quartz tube under Ar during all heat treatments. Differential scanning calorimetry (DSC) was performed using a TA Instruments Q100 V9.9 with heating and cooling rates of 10 °C/min between −180 °C and 150 °C.

Conventional, high-resolution and high angle annular dark field scanning TEM (HAADF-STEM) were used for characterization of the aged NiTiHf sample using an FEI Talos TEM (FEG, 200 kV). Additionally, a Titan G2 80–200 with ChemiSTEM technology using four embedded Bruker SDD detectors was also used for high spatial resolution energy-dispersive X-ray spectroscopy (EDX) mapping. A Fischione automatic twin-jet electropolisher (model 120) at 13 V was used to make a thin TEM foils from 90 to 100 μm grinded foils. An electrolyte of 30% HNO_3 in methanol (by volume) at around −35 °C was used for electropolishing.

The DSC measurement was performed on a $Ni_{50.3}Ti_{41.2}Hf_{8.5}$ sample after aging at 550 °C for 3.5 h. The transformation temperatures were:

* Corresponding author.
E-mail addresses: baminahmadi@mines.edu, behnam.aminahmadi@gmail.com (B. Amin-Ahmadi).

https://doi.org/10.1016/j.scriptamat.2018.09.019
1359-6462/© 2018 Acta Materialia Inc. Published by Elsevier Ltd. All rights reserved.

M_s (Martensite start temperature) = − 8°C, M_f (Martensite finish temperature) = − 75°C, A_s (Austenite start temperature) = − 19°C and A_f (Austenite finish temperature) =47°C. Therefore, after cooling from the final heat treatment, the sample would be expected to consist of an austenite matrix containing nano-sized H-phase precipitates. This was confirmed by bright field (BF) micrograph as shown in Fig. 1(a). The corresponding selected area electron diffraction (SAED) pattern is also shown in the inset of the figure. The main spots in the SAED pattern belong to the B2 cubic austenite structure, and the super reflections at 1/3 positions along $\langle 110\rangle_{B2}$, indicated by arrowheads, are reflections from uniquely oriented H-phase precipitates. The lenticular precipitates embedded in the austenite matrix were 105±5 nm long and 24±1 nm wide.

Further characterization showed the existence of martensite (Fig. 1 (b)) in some regions of the same sample. Considering the DSC results, it is evident that partial martensite transformation occurred while electropolishing the TEM sample, which was carried out at −35°C, a temperature between M_s and M_f. Because A_f=47°C, which is warmer than the room temperature, some of the martensite was thermodynamically stable and did not transform back to austenite when the sample was heated back to room temperature after electropolishing.

The formation of such large, preferentially-oriented martensite lath structures, as opposed to randomly oriented collections of twins of self-accommodated martensite that usually form during cooling without an external stress [23], is attributed to mechanical (stress relaxation) effects in the TEM foil during transformation. Stress relaxation effects in thin foil plan view TEM specimens have been studied using finite element analysis [24]. The stress can originate from lattice mismatch [24] and heterogeneity in stress distribution [25]. Abnormal stress-induced grain growth in nanocrystalline metals was also observed due to stress relaxation in TEM samples [25]. In the present NiTiHf sample, cracks were also observed, providing further evidence for local mechanical stresses in the sample, most likely due to lattice mismatch between the austenite and nano-H-phase precipitates [26] and internal stress heterogeneities inherent to nano-scale samples [27,28].

Fig. 2 shows a BF micrograph of one of the observed cracks. This condition provided opportunity to study crack propagation mechanisms. The crack initiated from the edge of the TEM specimen hole (upper right corner of Fig. 2(a)) and propagated through the martensite phase and finally entered and arrested in the austenite phase. Fig. 2

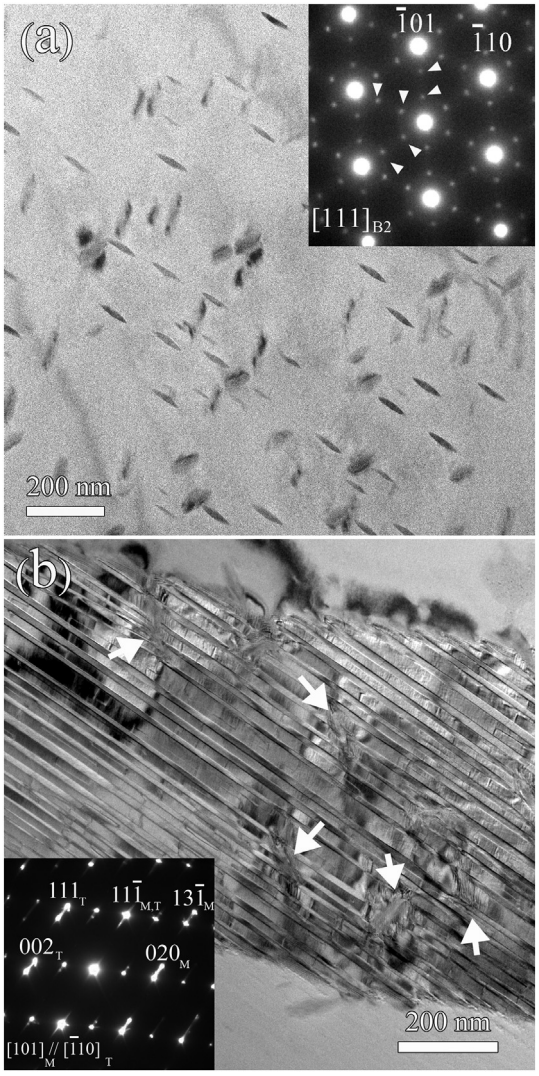

Fig. 1. (a) conventional BF micrograph of $Ni_{50.3}Ti_{41.2}Hf_{8.5}$ sample after aging at 550 °C for 3.5 h. The corresponding SAED pattern along the $[111]_{B2}$ zone axis is presented in the inset, with H-phase super reflections indicated by arrowheads. (b) A BF-TEM micrograph and corresponding SAED from the of the same sample taken along $[101]_M // [\bar{1}10]_T$ showing the presence of B19′ monoclinic martensite phase with ⟨011⟩ type II twin structures.

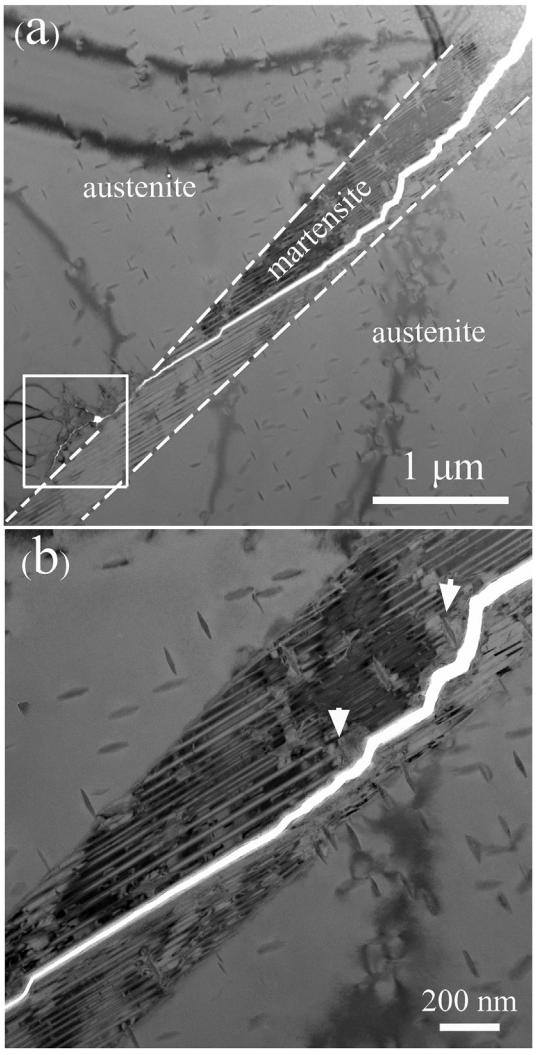

Fig. 2. (a) conventional BF micrograph showing a crack within the martensite phase of the NiTiHf alloy and (b) high magnification BF image showing the crack path along ⟨011⟩ type II twin planes. The crack is interrupted when it encounters H-phase precipitates (indicated by white arrows) and redirected to another twin boundary creating a torturous crack path.

(b) shows that the crack propagated along the ⟨011⟩ type II twin planes. It is generally known in other alloy systems that twin boundaries can act as an easy path for the propagation of cracks, limiting ductility [29]. However, in the present case, the crack propagates in a zig-zag manner between different twin planes. Trace analysis indicated that the path the crack takes between different ⟨011⟩ type II twin planes, to avoid the H-phase precipitates, is not an orientation that aligns with known martensite twin planes. Thus, it can be inferred that the H-phase precipitates (shown by white arrows in Fig. 2(b)) and their corresponding elastic strain fields [26] act as a barrier against crack movement, causing the crack to deflect and take a more torturous path through the monoclinic crystallites.

These observations provide insights concerning possible strategies for improving the fracture behavior of the martensite in NiTiHf SMAs. Most obviously, a denser distribution of larger (100–200 nm) H-phase precipitates would likely improve the fracture toughness of martensite. Because the cracks prefer to follow twin interfaces rather than take a more general intragranular path through the martensite phase, the energy required for fracture along twin interfaces is apparently much lower than intragranular fracture of the martensite. Therefore toughening could be realized by forcing more intragranular fracture and by creating a longer and more torturous crack path. This could be accomplished by introducing a higher density of H-phase precipitates of the size observed in this study, which act as obstacles to crack motion increasing the overall fracture toughness of the martensite. Moreover, formation of smaller martensite laths of many orientations can also prohibit crack propagation via regular interruption of twin interfaces, again increasing the length of crack paths. This toughening strategy is similar to the effect observed in metallic systems prone to intergranular fracture where decreasing the grain size is used to improve fracture toughness [29].

Fig. 3(a) shows a dark-field (DF) micrograph of the tip of the crack, which is within the austenite phase at the time of the observation (indicated by the white box in Fig. 2(a)). In order to observe any possible stress-induced martensite around the crack tip, the neighboring martensite lath was tilted to the $[\bar{1}10]_{B19'}$ zone axis and the associated diffraction spots were used to form the DF images shown in Fig. 3(a) & (b). The $(111)_{B19'}$ diffraction spot (marked by white circle) was used to form the DF image of Fig. 3(a). It is apparent that several nanosized martensite plates are present along the edge of crack inside the austenite phase (indicated by white arrows in Fig. 3(a)). The martensite is most likely retained due to stress concentrations about the crack tip. TEM analysis showed that the crack tip was sharp and did not exhibit dislocation activity that would lead to crack tip blunting [30].

Moreover, the SAED pattern of Fig. 3(a) shows diffuse intensity halos, indicating the existence of amorphous phase. The enlarged DF image (Fig. 3(b)) shows that the amorphous phase is present along the edges of the crack as well as in the region ahead of the crack tip itself. Fig. 3(c) exhibits a HRTEM micrograph of a region around the crack edge within the austenite. The amorphous layer can be seen. In addition, some nano-crystals were also observed within the amorphous matrix, as indicated by white arrows in Fig. 3(c).

While the crystals are too small to definitively determine their crystal structure, the morphology suggests that they are nucleated, twinned martensite. Similar nano-crystal formation during cold-rolling experiments in NiTi has been also reported [31] and related to the dislocation accumulation in the crystalline phase. However in the present study, dislocation accumulation at or near the crack tip was not observed. Therefore, another mechanism would have to be responsible for nanocrystal formation around the crack edge, such as stress-induced nanodomains (similar to Fig. 3(a)) or a local melting process and subsequent rapid cooling [32]. The twinned martensite-like morphology of the nanocrystal suggests the former mechanism. So, based on HRTEM observations, the stress concentration at the crack tip within the austenite matrix can generate three different types of damaged regions including amorphous, amorphous + nanocrystals, and crystalline (due to stress induced martensite inside an austenite grain), consistent with a previous report in a binary NiTi sample [33].

Amorphization about the crack edge was also observed in regions of the crack situated in the martensite phase (Fig. 3(d)). In this case, however, nanocrystals were not observed around the crack edge. The diffuse ring in the corresponding FFT (inset of Fig. 3(d)) confirms the existence of a predominantly amorphous phase, suggesting that different from the previous study on binary NiTi [33], in this sample, an amorphous + crystalline region is not observed about the cracked martensite. The observation of martensite-like nanocrystals in the amorphized austenite, but the lack of such crystals in the amorphized martensite further supports the inference that the nanocrystals are stress-induced martensite.

Having discussed the mechanisms for formation of nanocrystals in the amorphous + crystalline region, we now turn our attention to the mechanism of amorphization. Monte Carlo simulations of face centered cubic materials suggest that the strain energy during crack propagation can be released by local melting at the crack tip below the thermodynamic melting temperature [34]. However, local stress-induced melting around a crack tip can be difficult to observe due to the existence of other energy dissipative processes such as dislocation emission from the crack tip, which lowers the stress levels, reducing the driving force for local melting. Furthermore, in these simulations, the liquefied crack tip region recrystallizes as the crack propagates to sustain the mechanical load, leaving no evidence that melting has occurred. Unlike the simulations, these experiments (Fig. 3) show clear microstructural

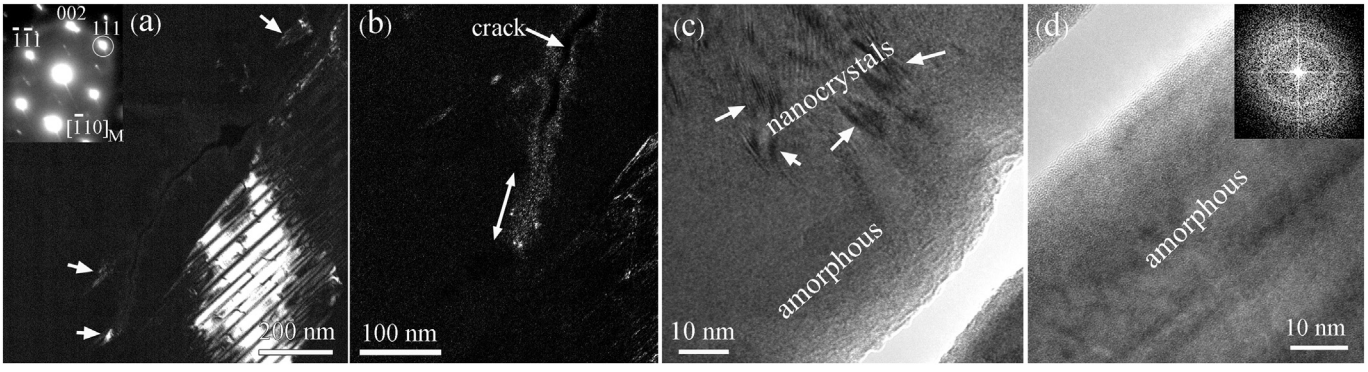

Fig. 3. (a) central DF micrograph imaged using g = $(111)_{B19'}$ showing the nano-sized stress-induced martensite formed inside the austenite phase near the crack edge. (b) magnified DF image around the crack tip highlighting structure in the amorphous diffraction condition. (c) HRTEM micrograph around the crack edge within the austenite phase, showing amorphous region immediately next to the crack, and formation of nanocrystals (indicated by white arrows) within the edge of the amorphous region. (d) HRTEM micrograph around the crack edge within the martensite phase showing the amorphous region, but the absence of nanocrystals.

evidence of melting at the crack tip in the form of a remnant amorphized region.

The amorphization around a crack tip can also be explained by disorder-driven glass formation due to large localized stresses driving the local material state far-from-equilibrium [33]. Analogous far-from-equilibrium amorphization has also been observed during irradiation with energetic particles at low temperatures [35–37] and radiation-induced amorphization is simply considered a disorder-induced melting of a critically-damaged crystal to a frozen supercooled liquid or so called glassy state [33]. In the current study, the measurement of the average amorphous region along the crack edge (20 nm) and amorphous region ahead of crack tip (80 nm shown by double arrowhead in Fig. 3 (b)) suggests that amorphization occurs before a crack propagates. STEM-EDX chemical mapping was also applied around the crack tip. The quantified EDX data showed the enrichment of Ni (around 25%) within the 20 nm amorphized vicinity of the crack edge. The Hf content did not change around the crack, but the same region was Ti-lean. It is already known that binary NiTi alloys can undergo a strain glass transition via excess Ni solute atoms (doping effect) that destroys the long-range strain order [38]. In the present work, it is difficult to definitively state which came first – the amorphization, or nickel diffusion to the high stress region about the crack tip, but the observation confirms that the two phenomena are coupled to the stress localization, and that the material first amorphizes, and then the crack propagates through the glass.

Finally, we address concerns that the observations reported in this work may be due to artifacts of the TEM experiments. Matsukawa et al. [35] used a high voltage electron microscope operated at 1 MeV and a focused electron beam of 2 μm to amorphize NiTi alloys. However, the electron microscope used in this work was operated at 200 KV and all the conventional and HRTEM images were taken using a wide and parallel electron beam (low electron dose). Therefore, electron beam irradiation induced amorphization is not responsible for the observations in the present study. The second concern may be if the mechanisms were thin-foil (thickness < 100 nm) effects. However, stress-induced martensite ahead of crack tips, with cracks propagating through the martensite has also been documented for thick samples, including the in situ X-ray diffraction study of Gollerthan et al. [30] in NiTi alloys. Thus, the mechanisms reported here are also expected in the bulk fracture of NiTiHf alloys.

In summary, the study of crack propagation through martensite in $Ni_{50.3}Ti_{41.2}Hf_{8.5}$ (at.%) showed that cracks propagate mainly along the ⟨011⟩ type II twin planes, zig-zagging between different twin planes to avoid H-phase precipitates. Stress-induced amorphization of the crack edge was also observed in both the austenite and martensite phases. A larger amorphous region ahead of crack tip compared with the amorphous region along the crack edge, suggests that amorphization occurs before the crack propagates. Ni enrichment by 25% around the crack tip confirms the amorphization mechanism is accompanied by a Ni doping effect, consistent with the motivating ideas of strain glass theory. One important follow-on study critical to further understanding the best microstructure engineering strategies for toughening is to document exactly how the sizes and coherency strain fields of H-phase precipitates interact with cracks, and to gain that understanding relative to cracks propagating through austenite vs. martensite structures. This work demonstrates that engineering H-phase precipitate morphologies is one viable path toward engineering the fracture toughness of NiTiHf alloys.

Financial support for this work was provided by the U.S. Department of Energy, Office of Basic Energy Sciences (grant no. DE-SC0010594). R.D.N. gratefully acknowledges support for making the materials and his participation in the publication from the NASA Transformative Aeronautics Concepts Program, Transformational Tools & Technologies (TTT) Project, and the SMA Technology Lead, Dr. Othmane Benafan.

References

[1] G.S. Bigelow, A. Garg, S.A. Padula, D.J. Gaydosh, R.D. Noebe, Scr. Mater. 64 (2011) 725.
[2] A. Evirgen, I. Karaman, R. Santamarta, J. Pons, R.D. Noebe, Acta Mater. 83 (2015) 48.
[3] J. Wang, H. Sehitoglu, Philos. Mag. 94 (2014) 2297.
[4] B. Amin-ahmadi, T. Gallmeyer, J.G. Pauza, T.W. Duerig, R.D. Noebe, A.P. Stebner, Scr. Mater. 147 (2018) 11.
[5] O. Benafan, R.D. Noebe, S.A. Padula, R. Vaidyanathan, Metall. Mater. Trans. A 43 (2012) 4539.
[6] A.P. Stebner, G.S. Bigelow, J. Yang, D.P. Shukla, S.M. Saghaian, R. Rogers, A. Garg, H.E. Karaca, Y. Chumlyakov, K. Bhattacharya, R.D. Noebe, Acta Mater. 76 (2014) 40.
[7] O. Benafan, A. Garg, R.D. Noebe, G.S. Bigelow, S.A. Padula, D.J. Gaydosh, N. Schell, J.H. Mabe, R. Vaidyanathan, Intermetallics 50 (2014) 94.
[8] O. Benafan, R.D. Noebe, T.J. Halsmer, S.A. Padula II, G.S. Bigelow, D.J. Gaydosh, A. Garg, Shape Memory and Superelasticity, 2, 2016 218.
[9] K. Bhattacharya, Oxford University Press, 2003.
[10] J.M. Ball, R.D. James, Arch. Ration. Mech. Anal. 100 (1987) 13.
[11] M.S. Wechsler, D.S. Lieberman, T.A. Read, Trans. AIME 197 (1953) 1503.
[12] G. Eggeler, E. Hornbogen, A. Yawny, A. Heckmann, M. Wagner, Mater. Sci. Eng. A 378 (2004) 24.
[13] R. Abeyaratne, S.J. Kim, Int. J. Solids Struct. 34 (1997) 3273.
[14] A.R. Pelton, J. Mater. Eng. Perform. 20 (2011) 613.
[15] A.R. Pelton, G.H. Huang, P. Moine, R. Sinclair, Mater. Sci. Eng. A 532 (2012) 130.
[16] A. Ahadi, Q. Sun, Scr. Mater. 113 (2016) 171.
[17] G.M. Loughran, T.W. Shield, P.H. Leo, Int. J. Solids Struct. 40 (2003) 271.
[18] S. Desindes, S. Daly, Int. J. Solids Struct. 47 (2010) 730.
[19] V. Di Cocco, F. Iacoviello, C. Maletta, S. Natali, Int. J. Fatigue 58 (2014) 136.
[20] T. Baxevanis, A.F. Parrinello, D.C. Lagoudas, J. Mech. Phys. Solids 89 (2016) 255.
[21] S. Hazar, W. Zaki, Z. Moumni, G. Anlas, Int. J. Plast. 67 (2015) 26.
[22] S. Hazar, G. Anlas, Z. Moumni, Int. J. Fract. 197 (2016) 99.
[23] M. Nishida, E. Okunishi, T. Nishiura, H. Kawano, T. Inamura, S. Ii, T. Hara, Philos. Mag. 92 (2012) 2234.
[24] R. Hull, Appl. Phys. Lett. 63 (1993) 2291.
[25] F. Wang, J. Zhao, P. Huang, A.S. Schneider, T.J. Lu, K.W. Xu, J. Nanomater. 1 (2013).
[26] B. Amin-Ahmadi, J.G. Pauza, A. Shamimi, T.W. Duerig, R.D. Noebe, A.P. Stebner, Scr. Mater. 147 (2018) 83.
[27] B. Amin-Ahmadi, D. Connetable, M. Fivel, D. Tanguy, R. Delmelle, S. Turner, L. Malet, S. Godet, T. Pardoen, J. Proost, D. Schryvers, H. Idrissi, Acta Mater. 111 (2016) 253.
[28] J.D. Giallonardo, U. Erb, G. Palumbo, G.A. Botton, C. Andrei, Mater. Sci. Forum 706–709 (2011) 1607.
[29] D. Althaf Basha, H. Somekawa, A. Singh, Scr. Mater. 142 (2018) 50.
[30] S. Gollerthan, M.L. Young, A. Baruj, J. Frenzel, W.W. Schmahl, G. Eggeler, Acta Mater. 57 (2009) 1015.
[31] J. Koike, D.M. Parkin, M. Nastasi, Philos. Mag. Lett. 62 (1990) 257.
[32] H. Ichinose, Y. Ishida, Scr. Metall. 19 (1985) 5.
[33] P.R. Okamoto, J.K. Heuer, N.Q. Lam, S. Ohnuki, Y. Matsukawa, K. Tozawa, J.F. Stubbins, Appl. Phys. Lett. 73 (1998) 473.
[34] R.M. Lynden-Bell, J. Phys. Condens. Matter 7 (1995) 4603.
[35] Y. Matsukawa, S. Ohnuki, J. Nucl. Mater. 239 (1996) 261.
[36] G. Thomas, H. Mori, H. Fujita, R. Sinclair, Scr. Metall. 589 (1982) 16.
[37] D.F. Pedraza, J. Mater. Res. 1 (1986) 425.
[38] Y. Wang, X. Ren, K. Otsuka, Phys. Rev. Lett. 97 (2006) 225703.